Dissociative Recombination of H_3O^+

Anthony E. Ketvirtis and Jack Simons*

Chemistry Department, University of Utah, Salt Lake City, Utah 84112

Received: April 5, 1999; In Final Form: June 21, 1999

Ab initio molecular orbital calculations have been performed on potential energy surfaces associated with products of dissociative recombination (DR) of $H_3O^+ + e^-$ experiments carried out in the ASTRID heavy-ion storage ring. Gradient geometry optimizations and frequency calculations on critical points on the H_3O ground-electronic-state surface and its dissociation paths were performed at levels of theory up to and including MP2(full)/6-311G(d,p) with extra diffuse functions added to the oxygen atom; single-point calculations subsequently were performed at levels up to CCSD(T) with the same basis set. Dissociation pathways of the two lowest-energy valence-to-Rydberg H_3O excited states were studied using CIS single-point calculations on SCF-level optimized geometries along ground-state H_3O dissociation pathways, and no barriers to fragmentation were observed. The most exothermic ground-state dissociation pathway connects H_3O to H_2O $(X^1A_1) + H$; however, $OH(X^2\Pi) + H_2$ and $OH(X^2\Pi) + 2H$ also are energetically accessible products. Dissociation of the two valence-to-Rydberg electronically excited H_3O species lead to these same products but also lead to products $(OH(A^2\Sigma) + H_2, OH(A^2\Sigma) + 2H)$ which are energetically inaccessible from ground-state H_3O. These computational results provide a detailed understanding of the intricacies of the observed experimental processes, and suggest future experimental investigations on the subject.

I. Introduction

The realm of gas-phase ion chemistry contains numerous classes of reactions responsible for the production of neutral molecular species. One widely studied reaction type has been dissociative recombination (DR), a process whose theory was treated by Bates and Massey in the 1940s.[1] The general form of DR, a reaction involving a molecular cation YZ^+ producing atomic or molecular products Y and Z, can be expressed as follows

$$YZ^+ + e^- \rightarrow Y + Z \qquad (1)$$

Depending on the manner in which the attaching electron enters an unfilled orbital of the YZ^+ cation, the DR processes are characterized in one of two classes:

(i) "direct,"[2] in which the cation YZ^+ captures an electron into an antibonding orbital, and the kinetic energy of the incoming electron provides sufficient energy to also excite electronically the initial cation electronic configuration. The resulting molecule, YZ**, is doubly electronically excited and is unstable with respect to autoionization, or, if the nuclei Y and Z separated to a distance ($r > r_{crit}$) such that autoionization is endothermic, the molecule becomes unstable to dissociation into Y and Z.

(ii) "indirect," [3] in which electron capture by YZ^+ occurs and the molecule goes into a high-energy Rydberg state $(YZ)_R$ lying below YZ^+ in electronic energy, but with excess vibrational and/or rotational energy. The resulting excited neutral molecule may autoionize or predissociate into a repulsive YZ state prior to dissociation into Y + Z, as is observed for the direct mechanism. (Both the direct and indirect cases are summarized in Figure 1.) The particular DR event considered in this paper, that involving $H_3O^+ + e^- \rightarrow H_3O$, is believed to proceed through the indirect mechanism for reasons that are made clear later.

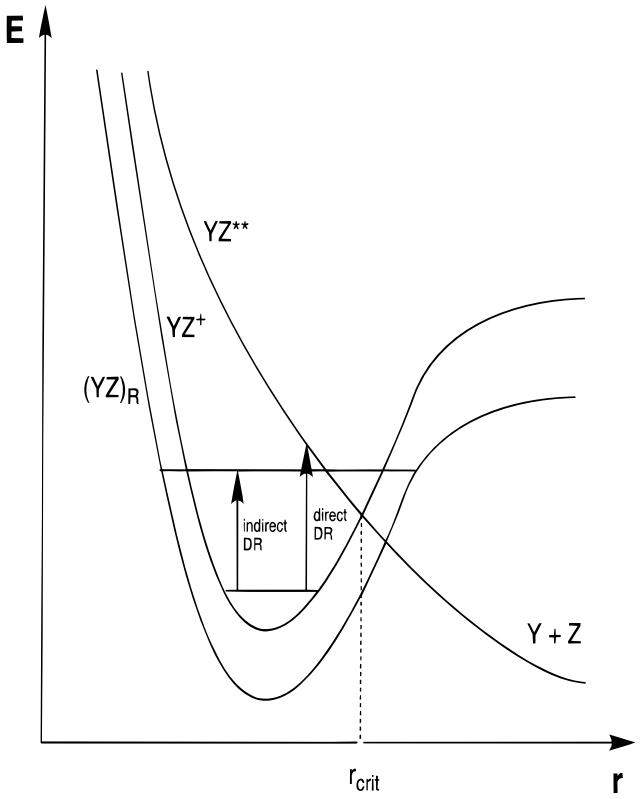

Figure 1. Direct and indirect dissociative recombination mechanisms.

A. Dissociative Recombination of H_3O^+. Dissociative recombination of H_3O^+ is believed to be important in the production of atoms, molecules, and radicals such as H, OH, and H_2O in diffuse and dense interstellar clouds.[4] The interstellar production of H_2O is of particular interest as it is an important

10.1021/jp991143e CCC: $18.00
Published on Web 08/03/1999

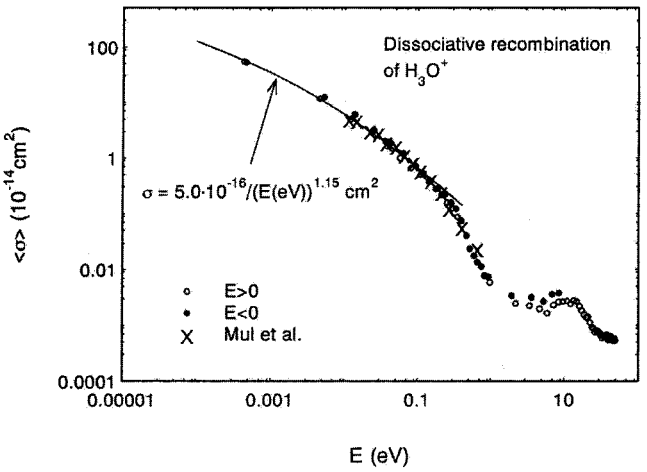

Figure 2. log−log plot of reaction cross-section vs relative beam energy for $H_3O^+ + e^-$ dissociative recombination as performed in the heavy-ion storage ring ASTRID (figure from ref 12q).

coolant in interstellar space and contributes significantly to star formation.[5]

Gas-phase studies of H_2O and H_3O^+ have been of considerable experimental interest during the preceding four decades, both from the perspective of proton-transfer reactions[6] as well as dissociative recombinations.[6s,7] Techniques employed to study such proton-transfer reactions include flowing afterglow[6a,7c,10d,e] and SIFT[6q,7c,10a−c,f−g] methods, as well as flame-ionization mass spectrometry,[6g,m−p,r−u] while DR reactions have been studied using the same methods,[7c,8,10a−c] as well as by laser-induced fluorescence,[7b,8,10c] vacuum UV absorption,[7b,8,9,10c] ion traps,[7d] merged ion-beam techniques,[7e−f,h−i] emission spectroscopy,[10c] flame-mass-spectrometry,[6s,7j−l] shock-tube techniques,[7m,n], flame-Langmuir probe techniques,[7v,10c] plasma-afterglow methods,[7w] glow-discharge methods,[7x] and heavy-ion storage rings.[11] The latter experimental technique represents a relatively recent innovation in the study of DR reactions; during the past decade, a plethora of experimental information regarding products and branching ratios of DR reactions has been obtained for ions which include H_2^+,[12a−h] HD^+,[12b,i] D_2^+,[12j] H_3^+,[12k,l] H_2D^+,[12l,m] $^3HeH^+$,[12n] N_2^+,[12o] O_2^+,[12o] NO^+,[12o] CH_5^+,[12p] H_2O^+,[12q] CH_3^+,[12q] and H_3O^+,[12q,r] the last of which is the subject of the present paper. In recent years, theoretical studies of dissociation pathways of H_3O^+,[13] as well as of predicted branching ratios of $H_3O^+ + e^-$ DR have been performed,[14] but there remain substantial discrepancies among the theoretical predictions (especially for branching ratios of various products) and experimental findings.

B. Overview of Heavy-Ion Storage Ring Experiments. In recent years, the experimental technique of using heavy-ion storage rings to study DR reactions has gained popularity.[7y,11a,b] There are four such ion-storage rings at which DR is studied: [7y,11a] ASTRID in Denmark,[11c] CRYRING in Sweden,[11d] TARN II in Japan,[11e] and TSR in Germany.[11f] With minor differences, each of these storage rings operates on a similar premise: Ions are produced from a parent neutral compound in an ion source; the resulting ion beam is accelerated to a desired translational energy and injected into a ring assembly under low-pressure conditions (on the order of 10^{-11} Torr). Such low pressures are required to allow the storage of the produced ion beam for time periods of the order of tens of seconds, and, thus, allow for radiative vibrational relaxation of the ions, as well as to prevent them from being dissociated by collisions with rest-gas molecules. Once inside the ring, the ion beam is manipulated by a series of radio frequency accelerators and bending and focusing magnets, to attain an ion beam of an appropriate energy such that the desired DR experiments can be performed.

The cold vibrational ion beam, then, is merged with a beam of electrons travelling in the same direction as the heavy ions with controlled relative kinetic energy in an "electron cooler." The beam relative energies can be controlled experimentally (and can, as will be discussed later, result in the formation of different products depending upon the relative beam energies). This type of "merged-beam" technique serves to provide a translational cooling mechanism for the stored ion beam, as well as to provide a venue for the DR reactions of interest to occur. The neutral products exit the storage ring in the direction of an energy-sensitive detector, at which a number of counts corresponding to the masses of each product particle is recorded. The resulting data is typically plotted in a log−log graph of reaction cross-section vs relative beam energy, from which rate coefficients (k) for the reaction or reactions under analysis can be obtained as follows. An example of such a plot of the cross-section for the formation of H_3O from H_3O^+ is shown in Figure 2.

$$k = \langle v\sigma \rangle = (N_{\text{signal}} v_i)/(N_{\text{ion}} n_e L \epsilon) \qquad (2)$$

In eq 2, N_{signal} is the number of particles detected per second for a given reaction channel (e.g., for H_3O formation in Figure 2), v_i is the heavy ion velocity, N_{ion} is the number of reactant ions which pass through the electron cooler per second, n_e is the electron density, L is the length of the electron cooler region, and ϵ is the detector efficiency.[12]

However, because the neutral products of the DR of a specific cation strike the detector within nanoseconds of each other (e.g., H_2 and OH formed from $H_3O^+ + e^-$ strike the detector together), this type of analysis by itself does not provide insight regarding the molecular structure of the products, because only one peak, corresponding to the mass, and hence the kinetic energy, of the undissociated molecule (H_3O in our case) can be expected to be seen. The installation of a grid with a known transmission (T) in front of the detector,[15] by contrast, allows such a peak to be separated into a series of peaks dependent upon the probability of product fragments (or combinations of fragments, such as H_2O, OH, OH + H + H, etc.) of given masses to go through (or to be stopped by) the grid. This separation is caused by the fact that, for example, H_2 + OH products pass through the grid with different probabilities than do H_3O or 2 H + OH products.

The number of "events" corresponding to products of a given mass striking the detector can be related to the branching ratio of the observed products through the matrix equation[12q] in which the probabilities of molecular passage through the grid relate the "known" raw data (the number of "hits" on the detector) to the "unknown" branching ratios. In this manner, the experimentalist gains valuable insight regarding the nature and the amount of products associated with DR of a given ionic species under analysis.

C. DR of H_3O^+. The storage ring method has been applied to study DR of H_3O^+. The primary results of the studies are the cross-sections for the total rate of production of neutral fragments from H_3O^+ (i.e., the total rate of loss of H_3O^+ through DR) and the branching ratios for production of various neutral products. Shown in Figure 2 is the H_3O formation cross-section, as a function of the relative kinetic energy of the two beams, for the H_3O^+ case.[12q] By determining, using the techniques discussed briefly above, how many H, OH, H_2O, and H_3O species reach the detector, these same experimental data have been used to determine the following branching ratios for H_3O

TABLE 1: Exponents of Augmented Basis Functions on Oxygen

s-functions	p-functions	d-functions
1.0	0.07983	0.084192
0.24474	0.024684	
0.059899		
0.014660		

decomposing in four reaction paths[12q,r]

$$H_3O^+ + e^- \rightarrow H_2O + H\ (0.33 \pm 0.08) \quad (3a)$$

$$OH + H_2\ (0.18 \pm 0.07) \quad (3b)$$

$$OH + H + H\ (0.48 \pm 0.08) \quad (3c)$$

$$O + H_2 + H\ (0.01 \pm 0.04) \quad (3d)$$

These branching ratios were obtained in collisions of low-energy electrons with H_3O^+ and hence they relate to the fate of H_3O produced at low energies.

The reaction cross-section vs relative beam energy plot reveals the presence of a smooth decay curve, characteristic of an endothermic reaction, punctuated by one or more undulations at high (ca. 2−10 eV) relative beam energies. While there is no doubt that the experimental information yields valuable insight regarding the products and branching ratios of the DR process, experimental limitations preclude a more detailed analysis of reaction mechanisms and determination of the electronic states in which products are formed. It is our belief that by examining the ground- and energetically-accessible excited-state potential energy surfaces connecting H_3O to its various decay products, we can gain a more profound understanding of the nature of the reaction(s) being studied, both from the perspective of reactants and of products. Our strategy, therefore, is to provide additional insight, via ab initio MO investigations, into the intricacies of the potential energy surfaces and the reaction mechanisms associated with the experimental observations, and, if possible, to provide suggestions regarding further experimental studies of this reaction.

II. Methods and Computational Strategy

A. Atomic Orbital Basis Sets. Our ab initio MO calculations were performed using the GAUSSIAN 94 series of programs,[16] on an IBM RISC System/6000 computer at the University of Utah. In all calculations, we have employed a standard Gaussian triple split-valence 6-311G(d,p)[17] basis set, augmented by a group of four extra sets of "s"-type functions, two extra sets of "p"-type functions, and one extra set of "d" -type functions on the oxygen atom. Many of these extra functions are diffuse, and assist in providing an accurate description of electrons which inhabit Rydberg orbitals. This extra group of basis functions was formed by modifying the set developed by Gutowski and Simons[18] for Rydberg neutral and anionic species by (1) retaining the basis functions necessary for a proper description of electrons in the low-energy Rydberg orbitals of interest (associated with electronic configurations of the ground state and two excited states of H_3O that relate to the features in Figure 2 near 10 eV noted above); yet (2) removing those functions which primarily describe higher-energy Rydberg orbitals. The final set of augmented primitive basis functions is detailed in Table 1.

To provide a pictorial representation of the occupied bonding σ_{OH}, nonbonding π_y, and Rydberg orbitals of the H_3O molecule, we have drawn these orbitals using the MOLDEN program.[19]

B. Geometry Optimization and Electron Correlation Issues. The ground electronic states of most species have been geometry optimized using gradient techniques[20] with this augmented basis set at levels of theory from Hartree−Fock (spin-restricted or RHF[21] for closed-shell species; spin-unrestricted or UHF[22] for open-shell species) and with inclusion of electron correlation to second-order Møller−Plesset perturbation theory[23,24] (RMP2(full) or UMP2(full), as appropriate), wherever possible. Transition structures have been located by gradient optimizations with the eigenvector-following (EF)[25] algorithm or the CALCALL[16] technique, and intrinsic reaction coordinate (IRC)[26] analysis was performed to verify the identities of the structures at the two ends (minima) of the associated reaction profiles. The total electronic energies given in Table 2 list MP2 energies for open-shell species without (UMP2) and with (PMP2) spin projection.[27] In addition, single-point calculations at the optimized MP2-level geometries have been performed at third-order (MP3(full))[23,28] and fourth-order (MP4(full))[23,29] Møller−Plesset theory (the latter energies are reported in Table 2 with inclusion of single, double, triple, and quadruple excitations (SDTQ)[29a,c]), as well as with coupled-cluster theory[30] with inclusion of single and double excitations, and perturbative inclusion of triple excitations (CCSD(T)(full)[30l−n]). All MP3 and MP4 energies of open-shell species are reported with inclusion of spin projection (PMP3, PMP4). Harmonic frequency calculations for species at critical points were performed on the respective UMP2 optimized geometries; from these calculations, zero-point vibrational energies (ZPE) also were obtained. ZPE values are reported in Table 2, scaled by a factor of 0.95.[31]

Energies of valence-to-Rydberg electronically excited states of H_3O, both pyramidal and planar (the significance of which will be explained shortly), have been obtained at the optimized ground-state HF-level geometries by single-point configuration interaction calculations which involve single electronic excitations (CIS).[32]

C. Characterization of Reaction Paths. *1. Ground-State Paths.* Our general strategy in studying how the ground and various valence-to-Rydberg excited states of H_3O connect to corresponding electronic states of $H + H_2O$, $OH + H_2$, and $OH + 2H$ products has been to first carry out searches on the ground electronic surface for reaction paths that pass through true transition states (i.e., minimum-energy cols where the gradient vanishes and where all but one eigenvalue of the curvature matrix are positive). This allows us to properly characterize the decomposition of ground-state H_3O in terms of reaction path energy profiles and corresponding transition-state energies and structures.

These searches were performed at the SCF level of theory, with the basis set described earlier. In the case of the reaction path which connects ground-state H_3O to $OH\ (X^2\Pi) + 2H$ directly, the emergence of severe spin contamination along this path compelled us to examine this route at a higher (QCISD(full))[16] level of theory, from which we also obtained PMP3 energies. The endothermicities for the reaction $H_3O \rightarrow OH\ (X^2\Pi) + 2H$ calculated at the QCISD and PMP3 levels of theory were in agreement to within 2 kcal mol^{-1}. As the energies at the latter level of theory had spin contaminants $(s + 1)$ to $(s + 4)$ removed and were reported at a pure doublet spin state ($\langle S^2 \rangle = 0.75$), we are confident in the reliability of these results at both levels of theory.

2. Excited-State Paths. For the valence-to-Rydberg excited states, we have had to take an alternative strategy in characterizing how the states of H_3O connect to those of $H + H_2O$, $OH + H_2$, and $OH + 2H$ because the states of interest are not the

TABLE 2: Total[a] and Relative[b] Energies of H_3O^+, H_3O, and Dissociation Products

	E (hartrees)[c,d]							
species	UHF[e]	$\langle S^2\rangle$ HF/**MP2**	UMP2[f]	PMP2[f]	PMP3[f]	PMP4 SDTQ[f]	CCSD(T)[f]	scaled ZPE[g]
1	−76.50716	0.752/**0.752**	−76.76875	−76.76906	−76.77280	−76.78423	−76.78415	15.77
4[h]	−76.50163	0.752/**0.752**	−76.77692	−76.76222	−76.76595	−76.77709	−76.77692	13.84
7	−76.33363			−76.57550	−76.58153	−76.58983	−76.58971	20.84
8	−76.05511			−76.30147	−76.30441	−76.31520	−76.30818	12.89
9	−0.49981	0.750						
10	−75.41631	0.756/**0.756**	−75.60634	−75.60803	−75.61768	−75.62356	−75.62334	5.20
11	−75.26086	0.760/**0.761**	−75.45369	−75.45618	−75.46406	−75.47074	−75.47035	4.53
12[i]	−1.13249			−1.16027	−1.16624	−1.16773	−1.16832	6.09[j]
13	−76.54910	0.756/**0.756**	−76.76730	−76.76898	−76.78465	−76.79205	−76.79242	12.33
14[h]	−76.50042	0.754/**0.755**	−76.76399	−76.76469	−76.76743	−76.77977	−76.77222	13.61
17[k]	−76.45643	0.758/**0.762**	−76.72819	−76.73062	−76.73322	−76.74859	−76.74744	11.46
18[h]	−76.51054	0.798/**0.781**	−76.75223	−76.75724	−76.76825	−76.77753	−76.77979	11.85

[a] In hartrees; ZPE not included. [b] In kcal mol^{-1}. [c] Spin-unrestricted formalisms are used for open-shell species; spin-restricted formalisms are used for closed-shell species. [d] All energies are reported using a 6-311G(d,p) basis set augmented by four extra sets of "s" functions, two extra sets of "p" functions, and one extra set of "d" functions on oxygen unless otherwise stated. See text for details. [e] Optimized at this level. [f] At optimized UMP2 geometries. [g] In kcal mol^{-1} at UMP2 optimized geometries unless otherwise stated; scaled by 0.95. [h] Transition structure. [i] 6-311G(d,p) basis set (no extra diffuse functions) was used. [j] In kcal mol^{-1} at UMP2(full)/6-311G(d,p)-optimized geometry; scaled by 0.94.[31] [k] Second-order saddle point.

lowest states of a given symmetry, so the quantum chemical tools available to us (e.g., analytical gradient and Hessians that are used to trace out reaction paths) are not able to generate true reaction paths on these excited states. To illustrate the difficulty, consider the situation at the starting geometry of the H_3O species, where the ground state is one in which the highest occupied orbital is the lowest-energy Rydberg orbital (R). The lowest excited states of this species involve promotion of the electron occupying R to other higher-energy Rydberg orbitals (R′). Even within our finite basis, there are fifteen such states lying below the $H_3O^+ + e^-$ threshold. These are not the states that are relevant to the undulations near 10 eV in Figure 2. Such R-to-R′ electronic promotions retain the monocationic character of the underlying cores and, in this manner, are not fundamentally different from that of ground-state H_3O. In contrast, excited states in which an electron is promoted from a valence orbital (e.g., from the nonbonding lone pair orbital on oxygen or from one of the OH σ bonding orbitals) into a Rydberg orbital while retaining another electron in R are the states that relate to the features in Figure 2. These excitations result in the creation of dicationic (H_3O^{2+}) cores (surrounded by two Rydberg electrons) in which the resulting Coulomb repulsions provide the driving forces toward subsequent prompt dissociation.[33] We believe that the undulations observed in Figure 2 are caused by the decomposition of such excited-state molecules, and the energies we obtain for such states support this postulate. By carrying out single-excitation configuration interaction (CIS) calculations with the ground state of H_3O as the reference state from which excitations occur and examining the orbital excitation nature of many eigenvectors of the CIS secular problem, we were able to identify the valence-to-Rydberg states of interest. Within our basis, at the geometry of ground-state H_3O, the two lowest such states were the 16th and 25th CIS states.

As mentioned earlier, the computational tools available to us do not allow us to compute true reaction paths for such states (i.e., the 16th and 25th roots). In particular, we have used the following strategy to characterize how these states and associated reaction paths evolve into $H + H_2O$, $OH + H_2$, and $OH + 2H$ products.

(a) Along each of the reaction paths that we found for connecting ground-state H_3O to $H + H_2O$, $OH + H_2$, and $OH + 2H$, we carried out CIS calculations from which we were able to identify, as detailed above, the valence-to-Rydberg states of interest.

(b) At each point along such paths, adding the CIS excitation energy of each such state to the energy of the ground-state species, we obtained an energy for the excited-state species.

(c) It is these excited-state energies that we depict in Figure 3, where we show how the electronic states of H_3O connect to those of $H + H_2O$, $OH + H_2$, and $OH + 2H$.

Although the resulting excited-state energy profiles do not represent how the state energies vary along the intrinsic reaction coordinates of the excited state, they still allow us to show how the ground and excited states of the H_3O reactants connect to those of the products. Moreover, because no barriers lying higher than the energies of the valence-to-Rydberg excited states at the H_3O geometry have been found along these profiles, we can be certain that no such barriers exist on the true intrinsic reaction paths of these excited states (because our CIS-computed excited-state energies must lie above the minimum-energy-path energies for these states).

Finally, when examining the ground-state reaction path (as well as the CIS excited-state profiles derived from it) for decomposition of H_3O to $H_2 + OH$, we employed an additional computational device. The ground-state hydronium radical, which we denote $(H_3O)_R$ to emphasize its outer Rydberg orbital, is pyramidal (C_{3v}), but possesses such a small inversion energy barrier (approximately 2.6 kcal mol^{-1}) that it is nearly planar. This feature of $(H_3O)_R$ allows us to investigate dissociation pathways of ground- and excited-state H_3O to produce $H_2 + OH$ by starting with the planar D_{3h} species which we denote $[(H_3O)_R]^‡$, (where ‡ denotes transition structure) and using both the plane of symmetry coincident with the molecular plane (σ'), as well as the symmetry plane which bisects the molecule through an O−H bond (σ), to label the symmetries of the orbitals and states. We thus first computed the energy of the state connecting $OH(^2\Sigma^+) + H_2$ with H_3O along a path that preserves both such symmetry planes; at each point along that path, the energies of the two states correlating to $OH(^2\Pi) + H_2$ were then obtained using CIS energy differences from this $OH(^2\Sigma^+) + H_2$ state. This procedure produced the data shown in Figure 3 as connections between $OH + H_2$ and H_3O that display crossings (near −62 kcal mol^{-1}) among these three diabatic states. If, as is almost certain under experimental conditions, the σ and σ' planes of symmetry are not operative, these three diabatic electronic states will undergo avoided crossings at this conical intersection region to yield the true adiabatic electronic states (i.e., the lowest curve shown in Figure 3 adiabatically

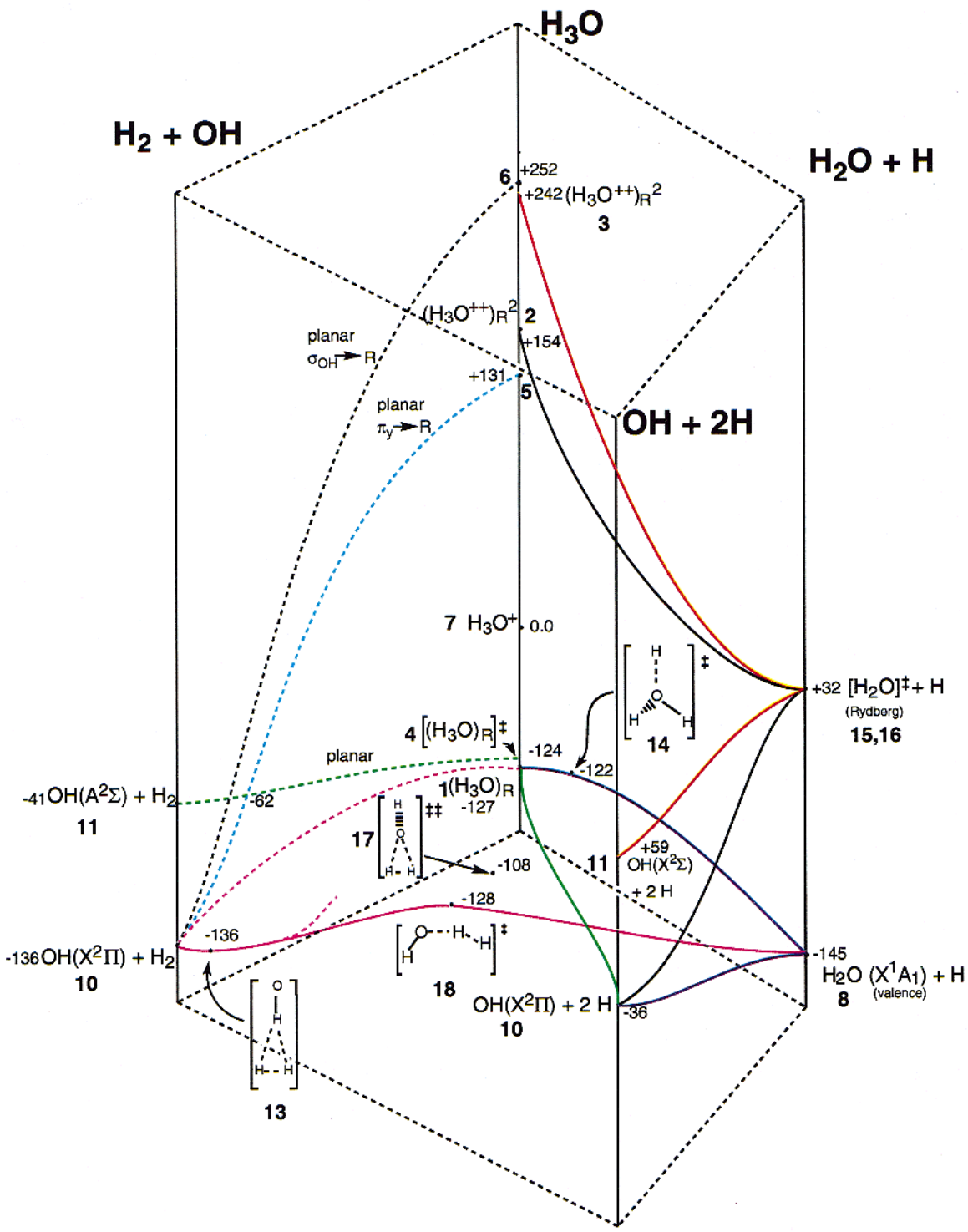

Figure 3. Dissociation pathways and energies of H_3O and dissociation products (H_2, OH) and (H_2O, H) relative to H_3O^+ in kcal mol^{-1}. Energies for all species are reported at CCSD(T)//UMP2 with the basis set described in Section II. A., except for **2**, **3**, **5**, and **6** (CIS//SCF), and **15** and **16** (CCSD(T)//SCF). Dissociation paths involving species **2**, **3**, **5**, **6**, **15**, and **16** were obtained from CIS single-point calculations along SCF ground-state reaction paths; the remaining paths were obtained as discussed in Sections II.B and II.C.

connects ground-state H_3O to OH($^2\Pi$) + H_2, the second curve connects the first valence-to-Rydberg state of H_3O to OH($^2\Pi$) + H_2, and the third curve connects the second valence-to-Rydberg state of H_3O to OH($^2\Sigma^+$) + H_2).

III. Results and Discussion

A. Structures and Relative Energies of Reactants and Products. Table 2 displays the total electronic energies (in hartrees) and zero-point vibrational energies (in kcal mol^{-1}) associated with the hydronium ion H_3O^+ (in essence, the initial "reactant" of the storage-ring experiments), with recombined H_3O, and with the various dissociation products H_2O, OH, H_2, and H, in various ground state, and electronically excited states. Pictorial representations of the optimized minimum-energy structures and transition structures are given in Figure 4, which we now briefly summarize.

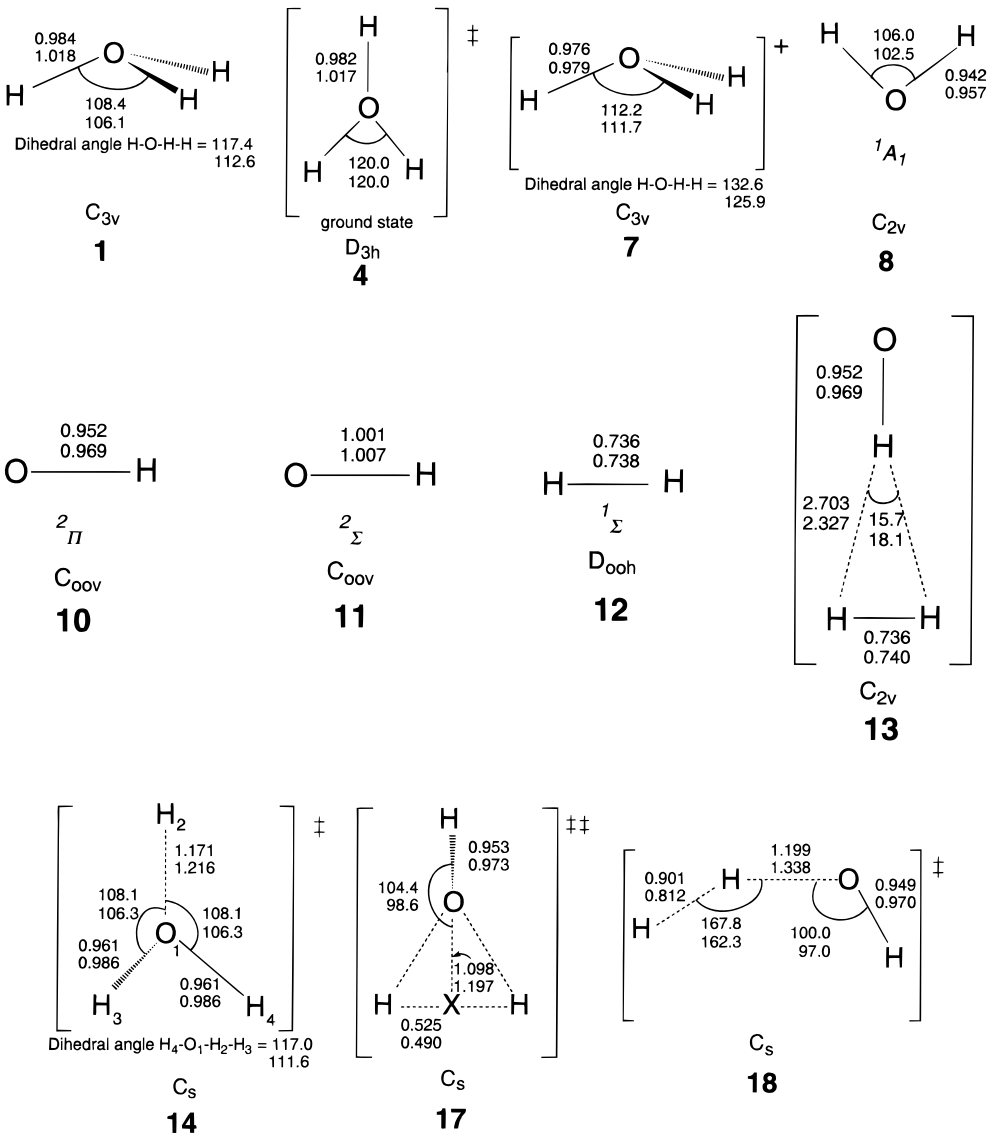

Figure 4. Structural parameters of H_3O^+, H_3O, and dissociation products. Bond lengths are in Ångströms; bond angles are in degrees. Where one set of geometric parameters is listed, it denotes an optimized structure at the HF/6-311G(d,p) level of theory. Where two sets of geometric parameters are listed, the upper value denotes optimization at the HF/6-311G(d,p) level of theory; the lower value denotes optimization at the MP2(full)/6-311G(d,p) level of theory. In each case, these basis sets have been augmented by four sets of extra "s" functions, two sets of extra "p" functions, and one set of extra "d" functions on oxygen.

Species **1** represents ground-state $(H_3O)_R$, a pyramidal C_{3v} structure which is believed to to the initial product of $H_3O^+ + e^-$ DR under ASTRID conditions at low relative beam energies (i.e., for energies below ca. 1 eV),[34] and is a species which has been the subject of previous theoretical[35] and experimental[36] research. The highest filled (singly occupied) molecular orbital of this species is the diffuse Rydberg orbital shown in Figure 5e.

Molecules **2** and **3** represent the electronically excited states of H_3O, which we believe relate to the features seen near 2−10 eV in Figure 2. Molecule **2** differs from **1** in its electronic configuration by a single electronic excitation from the nonbonding lone pair (π_y in Figure 5c) to the aforementioned Rydberg orbital R. Molecule **3** differs from **1** by a single excitation from one of the doubly degenerate O−H bonding orbital pair ($\sigma_{OH(1)}$ or $\sigma_{OH(2)}$ in Figure 5a,b, respectively) to the R orbital. As species **2** and **3** represent electronically excited states of **1** obtained by CIS single-point calculations at the optimized geometry of **1**, the excited species are not depicted in Figure 4, although their (vertical) energies are shown in Figure 3, which summarizes the energetics of all species studied here.

Species **4** is the planar (D_{3h}) version of molecule **1**, which we denote $[(H_3O)_R]^‡$. As mentioned earlier, the low inversion barrier associated with the interconversion of equivalent forms of **1**, through **4**, allows us to use **4** in the study of the H_2-dissociation pathways of ground- and excited-state H_3O species. Analogous to species **2** and **3**, molecules **5** and **6** represent electronically excited states of **4** obtained by CIS single point (i.e., vertical) calculations on **4**.

Species **7** represents ground state cation H_3O^+, the initial reactant in the ASTRID DR experiments.[12q,r] This species has been studied extensively in many contexts.[6,7,12q,r,18,33a,37] Its structure is pyramidal with C_{3v} symmetry, and differs in electronic configuration from that of **1** only by the absence of an electron in a diffuse Rydberg orbital R.

Species **8** is the ground state of the water molecule (X^1A_1). Together with atomic hydrogen (species **9**), it represents one

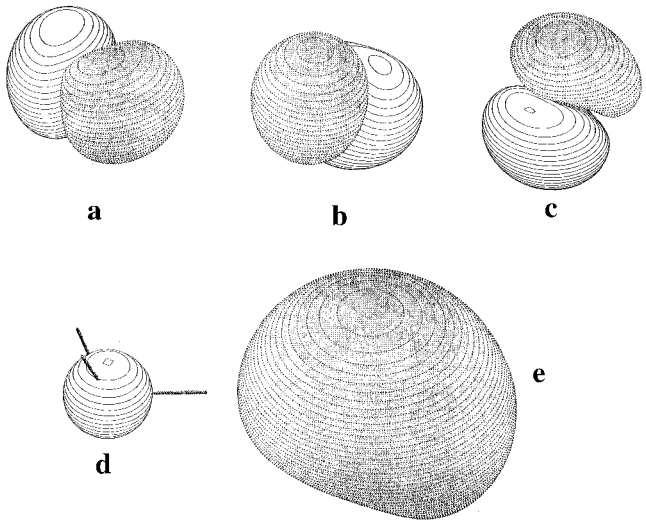

Figure 5. MOLDEN pictorial representations of occupied (a) $\sigma_{OH(1)}$-orbital, (b) $\sigma_{OH(2)}$-orbital, (c) π_y-orbital, (d) core (oxygen 1s) orbital, (e) Rydberg orbital in $(H_3O)_R$. Figure 5d is magnified by a factor of 2 relative to Figures 5a−c,e.

of the major products of $H_3O^+ + e^-$ DR as observed experimentally (see eq 3a).[12q,r]

Structures **10** and **11** represent OH radicals, in the ground-($X^2\Pi$) and lowest electronically excited ($A^2\Sigma$) states, respectively. The degenerate ground state of OH corresponds to an electron configuration in which an unpaired electron occupies an in-plane π-orbital (π_x) or an out-of-plane π-orbital (π_y); the excited $^2\Sigma$ state has the unpaired electron occupying a σ-orbital (σ_z).

The products $OH + H_2$ (species **12**) and OH + 2 H, corresponding to (3b) and (3c), represent nearly two-thirds of the observed $H_3O^+ + e^-$ DR products under ASTRID conditions.[12q,r] Structures **13** to **18**, which represent transition structures and reaction intermediates along the studied reaction pathways, will be discussed in the following section.

B. Structures and Relative Energies of Transiton States and Intermediates. Structure **13** is a loose van der Waals complex between $OH(X^2\Pi)$ (species **10**) and H_2 (**12**) in which the two constituent molecules are oriented perpendicularly with the H atom of OH directed toward H_2. This complex occurs in a shallow minimum along the well-studied H-abstraction reaction path between $OH(X^2\Pi)$ (**10**) + H_2 (**12**) and $H_2O(X^1A_1)$ (**8**) + H (**9**),[38,39] and lies 0.43 kcal mol^{-1} below OH + H_2 (optimized at UMP2 without zero-point vibrational energy (ZPE)). On inclusion of ZPE (without the energy contribution of the $OH\cdots H_2$ symmetric stretching frequency) at the same level of theory, **13** lies 0.41 kcal mol^{-1} above OH + H_2 (at our highest level of theory (CCSD(T)//UMP2 with the basis set described in section II), **13** lies 0.36 kcal mol^{-1} above OH + H_2 with ZPE included). However, as **13** has been isolated experimentally[40] and has been the subject of previous theoretical studies,[40a,c,41] our results suggest that even our highest level of theory is inadequate to provide a proper description of this very weakly bound complex. Nevertheless, it is highly unlikely that **13** will be formed in the $H_3O^+ + e^-$ DR process under ASTRID conditions.

Species **14** is the transition state for the dissociation of ground-state $(H_3O)_R$ (**1**) into ground-state H_2O (X^1A_1) (**8**) and a hydrogen atom (**9**), as shown in the blue curve in Figure 3. The barrier to this dissociation is small (5.33 kcal mol^{-1} at CCSD(T)//UMP2) and, as **14** is closer to the reactant neutral than to the products in energy, it is not surprising that **14** resembles **1** more closely in structure, as suggested by the Hammond postulate[42] (in particular, the separation between the oxygen atom and the departing H atom is only 0.198 Å longer in transition structure **14** than in minimum structure **1** as optimized at UMP2).

Our investigations of the dissociation pathways of **2** and **3** indicate the occurrence of single hydrogen atom ejections, without barrier, to form products of stoichiometric formulas H_2O + H, with an electron occupying a diffuse Rydberg orbital in each H_2O species (**15** and **16**). These ejections are followed by additional single H losses from each species to produce OH ($X^2\Pi$) + 2H and OH($A^2\Sigma$) + 2H, respectively. In attempting to study the H_2O species resulting from the initial H ejections, we were unable to locate any at local minima on the respective energy surfaces. However, on enforcing linearity, as a computational device, we have been able to study species with the electron occupancies of **15** and **16**, and, thus, gain insight into details of the dissociation pathways connecting electronically excited states of H_3O with H_2O + H and OH + 2H.

Species **15** and **16** represent electronically excited states of H_2O (**8**), and occur along paths connecting excited states of H_3O (species **2** and **3**, respectively) to H + H_2O, and subsequently to 2 H + OH. If we constrain **15** and **16** to be linear and use C_s point group notation, we can designate the unpaired valence electron in **16** to lie in an "in-plane" (a′) nonbonding orbital, and designate that of **15** in an "out-of-plane" (a″) nonbonding orbital; thus **15** has (^{1}A″) symmetry, and **16** has (^{1}A′) symmetry.

At nonlinear geometries, species **15** differs from ground-state **8** by the excitation of an electron from the nonbonding lone pair in an out-of-plane π-orbital (of b_1 symmetry) in **8** to a diffuse Rydberg orbital and **16** differs from **8** by the excitation of an electron from the in-plane (a_1-symmetry) nonbonding orbital to a diffuse Rydberg orbital. If linearity is imposed, however, the electronic occupancies of **15** and **16** become equivalent and thus these two states are degenerate. Moreover, under the constraint of linearity, these two degenerate species dissociate to the same ($OH(X^2\Pi)$ + H) products, whereas the closed-shell *linear* H_2O species (linear **8**) correlates with OH-($A^2\Sigma$) + H. However, on attempting to locate a linear local minimum structure with an electron occupancy as described for the degenerate pair, we first obtained a $D_{\infty h}$ structure ($r_{(OH)1} = r_{(OH)2} = 1.237$ Å) for which instability associated with the lone imaginary asymmetric stretch vibrational frequency (3178 cm^{-1}) led to decomposition into $OH(X^2\Pi)$ + H. Along such an enforced collinear dissociation path, however, the doubly degenerate pair and the linear closed-shell species experience a crossing near $r_{(OH)1} = 1.197$ Å, $r_{(OH)2} = 1.237$ Å where the closed-shell state falls below the degenerate pair; another energy crossing occurs near $r_{(OH)1} = 0.952$ Å, $r_{(OH)2} = 1.937$ Å, where the closed-shell state moves above the other two states and evolves to $OH(A^2\Sigma)$ + H. That is, as $r_{(OH)2}$ is lengthened beyond 1.937 Å, the degenerate pair correlates with $OH(X^2\Pi)$ + H, and the linear closed-shell species correlates with $OH(A^2\Sigma)$ + H.

While the symmetry label distinction between **15** and **16** is not essential at linear geometries, it becomes important on bending the H−O−H angle from 180°. Species **15** and **16** become nondegenerate, and **16** undergoes an avoided crossing with **8** near $r_{(OH)1} = 0.952$ Å, $r_{(OH)2} = 1.937$ Å where both have A′ symmetry. Thus, **8** correlates adiabatically with $OH(X^2\Pi)$ + H, whereas **16** correlates with $OH(A^2\Sigma)$ + H, as shown in

Figure 3. Species **15**, being of A″ symmetry, correlates with $OH(X^2\Pi) + H$, as noted earlier, and is unaffected in this regard.

Species **17** is a second-order saddle point on the ground-state H_3O surface that was obtained in our attempt to locate a transition structure along a path leading to symmetric dissociation of two H atoms from species **1**; this species also has been the subject of previous theoretical research.[35] The structure of **17** consists of an intact OH moiety, with the oxygen atom participating in a loose three-membered ring complex with the two "leaving" hydrogen atoms; the optimized geometry (O−H 1.293 Å; H−H 0.980 Å at UMP2) suggests that no strong OH or HH bonds exist in this ring structure. The two imaginary vibrational frequencies calculated at the UMP2 level of theory (2110i cm^{-1} and 1150i cm^{-1}) correspond to, respectively, an asymmetric O−H stretch and a symmetric O−H stretch-scissor motion, both of which involve motions of the "departing" hydrogen atoms.

The significance of **17** in the present context is only peripheral because it is neither a stable structure nor a first-order saddle point.

We also studied the path for the hydrogen abstraction reaction $OH(X^2\Pi) + H_2 \rightarrow H_2O\ (X^1A_1) + H$ (see the solid magenta line in Figure 3) and found the transition state **18** along this path. As this abstraction reaction has been the subject of previous experimental[38]and theoretical[38a,39] study, it is not surprising that **18** has been identified previously.[38a] Subsequent experimental[40] and theoretical[40a,c,41] studies resulted in identifying the loose van der Waals complex (**13**) in a very shallow minimum near the $OH(X^2\Pi) + H_2$ end of the pathway. We attempted to characterize the full IRC that connects $H_2O + H$, through **18**, further to **13**, and onward to $OH(^2\Pi) + H_2$. We succeeded in generating this IRC from **18** to $H_2O + H$, but our attempts to reach species **13** were not entirely successful. In particular, our IRC reached an energy very close to that of **13** and produced a structure having O−H and H−H bond lengths nearly identical to those found in **13**. However, the precise T-shaped orientation of the O−H and H−H bonds found in **13** could not be reached using Gaussian's IRC algorithm.

Finally, we attempted to find and characterize a transition state and a reaction path connecting ground state $(H_3O)_R$ **4** directly to ground-state $OH + H_2$ (**10**) by following the lower-energy sheet of the avoided crossing (see section II.C.2) shown at the left extreme of Figure 3. All attempts along these lines failed. We therefore decided to explore whether the reaction path discussed above connecting $H_2O + H$ to $OH + H_2$ through TS **18** undergoes a bifurcation that could offer a connection to $(H_3O)_R$. By carefully following the intrinsic reaction path from **18** toward $OH + H_2$, we were able to identify a region within which one of the eigenvalues of the mass weighted Hessian matrix (which gives the curvature of the energy surface) transverse to the reaction path evolved from positive, to negative, and back to positive. This behavior is indicative of a bifurcation of one "streambed" into two. The geometry in this region corresponded to essentially intact OH ($X^2\Pi$) and H_2 moieties, with the closest H atom in H_2 2.0 Å from the O atom; the energy at this geometry was closer to that of $OH + H_2$ than to that of **18**, and thus (see Figure 3) below the energy of H_3O. Unfortunately, our attempts to "walk" uphill along this new streambed were not successful (although we show in Figure 3, as a dashed magenta line, an abbreviated path corresponding to this second streambed).

Nevertheless, we believe we have been able to relate H_3O to $OH + H_2$ via a lower energy route than that discussed in section II.C.2. By starting at a point (X) having planar geometry along the reaction path which diabatically connects **4** with $OH(^2\Sigma) + H_2$ (dashed green line; see Figure 3) near the conical intersection with the path connecting **5** with $OH(^2\Pi) + H_2$ (dashed blue line) and distorting the molecule slightly to remove the σ and σ' planes, we have been able to perform subsequent geometry optimizations which lead either to **1** or to $OH(^2\Pi) + H_2$. Although we have been unable to locate an intrinsic reaction coordinate path between these two sets of minima, and thus, cannot state the barrier height of this process with certainty, we estimate an upper bound to be approximately 34 kcal mol^{-1} (the energy of a point obtained by applying an out-of-σ'-plane distortion to the point X and seeking a minimum along such a distortion). The route we arrived at connecting **1** to $OH(^2\Pi) + H_2$ is shown as the full dashed magenta line in Figure 3. Because the focus of the present effort is on interpreting data that occurs at energies above that of H_3O^+, the failure to fully characterize this particular branch of the ground-state surface is unfortunate but not limiting.

C. Energetic Accessibilities of Ground- and Excited-State Reactants. The reaction cross-section for $H_3O^+ + e^-$ recombination as studied by Andersen and co-workers[12q] reveals a diminishing cross-section with increasing relative beam energy up to approximately 2−10 eV, where one or two undulations are observed. Such features may suggest the formation, at higher energies, of electronically excited H_3O. In particular, we suggest later that these features relate to our species **2** and **3**, which are valence-to-Rydberg excited states of $(H_3O)_R$.

It is believed that when the relative energy of the reactant ion beam and the electron beam is low, one obtains (primarily) electronic ground-state recombination products[34] (e.g., $(H_3O)_R$) prior to dissociation. This, in turn, suggests that molecule **1** is of principal importance as the starting point in the examination of subsequent dissociations at low collision energy. Nevertheless, it must be remembered that even for low-energy DR, any products lying below the cation energy can be formed and thus must be considered.

If the relative electron-beam to ion-beam energy lies in the region where the undulations appear in Figure 2, it is thought that the production of ground-state H_3O diminishes in favor of the production of valence-to-Rydberg electronically excited H_3O, which, in turn, results in possible access to higher-energy dissociation products. Figure 3 shows one such electronically excited state of H_3O ($\pi_y \rightarrow$ R) (species **2**) to lie 281 kcal mol^{-1} above that of ground-state $(H_3O)_R$, and a second such excited state ($\sigma_{OH(1)} \rightarrow$ R or $\sigma_{OH(2)} \rightarrow$ R) (**3**) to lie 369 kcal mol^{-1} above ground-state H_3O. These two states lie 6.7 and 10.4 eV above the energy of the cation, respectively, and hence fall in the region where the undulations are seen in Figure 2. Experiments performed at sufficiently high relative beam energies may result in the production of such excited-state recombination products, and may account for the observed undulations in the experimental cross-sectional curve. Our ab initio studies of the associated potential energy surfaces provide an opportunity to suggest the fates of these "recombined" H_3O species, as will be presented in the next section of this paper.

D. Theoretical Interpretation of Experimental Results. *1. Low-Energy Collisions Producing Ground-State H_3O.* As can be seen in Figure 3, dissociative recombination of H_3O^+ can lead to a variety of final products, such as those observed in the ASTRID experiments.[12q,r] Clearly, the experimental results provide valuable information regarding the branching ratios of the DR reactions under investigation; however, they are limited in their specificity of information regarding product electronic states, product molecular structures, and reaction pathways. The

results of our computational investigation lend greater insight into these issues, a discussion of which follows forthwith.

Figure 3 illustrates the various accessible reaction pathways associated with DR of H_3O^+. At low (electron-beam to ion-beam) relative energies, it is suggested that DR of H_3O^+ results in the formation[34] of a neutral H_3O radical (denoted $(H_3O)_R$). This species possesses an unpaired electron in its highest-filled (Rydberg) orbital, which is depicted in Figure 5e, and is pyramidal (C_{3v}) in geometry, but has a low barrier (2.61 kcal mol^{-1}; see Table 2) to planarity. The presence of 127 kcal mol^{-1} excess internal energy from the exothermic electron capture allows $(H_3O)_R$ to dissociate via several reaction pathways. The most exothermic route involves the loss of a hydrogen atom to form ground-state H_2O (X^1A_1) ($\Delta E = -17.84$ kcal mol^{-1}), as shown on the solid blue path in Figure 3. Only a small barrier associated with O−H dissociation (5.33 kcal mol^{-1}) is encountered on this path; the existing 127 kcal mol^{-1} of excess energy from the initial electron−ion recombination reaction renders such a barrier insignificant.

Although the $(H_3O)_R \rightarrow H_2O$ (X^1A_1) + H reaction pathway is the most exothermic of all ground-state routes currently under study, it does not account for the largest fraction of products in the low-energy branching ratio analysis of the associated heavy-ion storage ring experiment (0.33 ± 0.08).[12q,r] The largest product channel in this regard (0.48 ± 0.08) corresponds to H_3O dissociation into OH + 2H.[12q,r] Therefore, it seems likely that both (a) enough energy remains in any H_2O ($^1A_1$) formed to permit subsequent fragmentation to OH ($X^2\Pi$) + H, and (b) direct fragmentation of H_3O to 2H + OH ($X^2\Pi$) (the solid green path in Figure 3) is significant. The use of theory in this regard thus allows the identification of the OH product electronic state in a manner which was not possible (or not considered) under experimental conditions.

Our theoretical studies also allow us to determine how $(H_3O)_R$ can decompose to OH + H_2. An examination of Figure 3 at first suggests a path connecting planar $[(H_3O)_R]^{\ddagger}$ (**4**) to OH($A^2\Sigma$) (**11**) + H_2 (**12**). However, as noted in section II.C.2, the presence of an avoided crossing of the $^2\Sigma$ and $^2\Pi$ diabatic curves lying 65 kcal mol^{-1} above $(H_3O)_R$ (thus still energetically accessible) predicts that the observed experimental product for ground state $(H_3O)_R$ should be OH($X^2\Pi$) + H_2. Although the precise reaction path connecting $(H_3O)_R$ to OH ($X^2\Pi$) + H_2 was, as noted in Sec. III. B, not fully characterized, it is shown in Figure 3 as a dashed magenta line. Of course, OH($^2\Pi$) + H_2 also can dissociate further, given the excess internal energy present, to produce OH($^2\Pi$) + 2H.

In summary, our energy surface shows that ground-state $(H_3O)_R$ can dissociate (a) to produce $H_2O(^1A_1)$ + H with enough internal energy to allow a fraction of the $H_2O(^1A_1)$ + H to undergo further decay to produce OH($^2\Pi$) + 2H; (b) to produce OH($^2\Pi$) + H_2 some fraction of which may fragment further to generate additional OH($^2\Pi$) + 2H; and (c) to produce OH($^2\Pi$) + 2H directly.

As the ASTRID experimental studies did not result in the observation of H_2 + O + H in significant quantities (branching ratio 0.01 ± 0.04),[12q,r] this reaction path was not considered in the present computational investigation.

The most straightforward use of these findings to interpret the branching ratios of eq 3 suggests that 18% of the $(H_3O)_R$ dissociates to H_2 + OH ($^2\Pi$) and 81% dissociates to H + H_2O ($^1A_1$) or directly to 2H + OH ($X^2\Pi$). Denoting as X the fraction of H_3O that follows the blue path to H_2O + H, and Y the fraction following the green path to OH + 2H, we have $XF = 0.33$ and $Y + X(1 - F) = 0.48$. Here F is the fraction of H_2O (X^1A_1) remaining intact, and thus (1 − F) is the fraction that proceeds on to OH + 2H. Clearly, the sum of the two branching ratios, $0.48 + 0.33 = 0.81 = X + Y$ depends on X and Y while each branching ratio also depends on F.

The findings discussed above relate to the *low-energy* DR because they derive from ground-state $(H_3O)_R$ and use branching ratios obtained at low energies.

2. Higher-Energy Collisions Forming Excited States of H_3O. The lowest-energy valence-to-Rydberg electronically excited state of H_3O (**2**) lying 6.7 eV above the H_3O^+ cation can be regarded as an H_3O^{2+} core surrounded by a doubly occupied diffuse Rydberg orbital, in which electronic excitation of ground-state H_3O from the nonbonding valence π_y orbital to a Rydberg orbital has occurred. At higher relative beam energies in the ASTRID apparatus, it is thought that this molecule may be formed as a recombination product rather than ground-state $(H_3O)_R$ (**1**). At still higher relative beam energies, it is thought that a higher-energy electronically excited H_3O species (a result of $\sigma_{OH(1)} \rightarrow$ Rydberg or $\sigma_{OH(2)} \rightarrow$ Rydberg excitation) (species **3**) may be formed on initial recombination prior to dissociation. In these states, one again has an H_3O^{2+} core surrounded by two Rydberg electrons. It therefore should come as no surprise that these energetic species undergo spontaneous dissociation, analogous to what occurs in doubly charged cations.[33]

a. The first valence-to-Rydberg excited state. As shown in Figure 3, species **2** lies approximately 281 kcal mol^{-1} above that of ground-state $(H_3O)_R$ (**1**) on the basis of our CIS calculations. The production of this ion in the initial electron−ion recombination process allows access to dissociation pathways which result in the formation of OH ($X^2\Pi$), either directly by H_2 loss (dashed blue line in Figure 3) or by sequential H atom losses (solid black line in Figure 3). (These results suggest that no intact H_2O should be formed in this case.) To the best of our knowledge, the branching ratios for OH + H_2 and OH + 2H have not been measured for this higher energy case. In the case of the direct H_2 loss mechanism, an initial examination of Figure 3 suggests a straightforward correlation between the (planar) lowest-energy valence-to-Rydberg excited H_3O (**5**) and OH ($X^2\Pi$) + H_2 via the dashed blue line. However, as was discussed earlier, the absence of molecular symmetry under experimental conditions and the associated avoided crossings result in the formation of OH ($X^2\Pi$) + H_2 via a slightly different route. In the absence of symmetry, the path follows the dashed blue line from **5** to the crossing with the dashed green line, then follows the dashed green line to its crossing with the dashed black line, and then follows the dashed black line to products OH ($X^2\Pi$) + H_2.

b. The second valence-to-Rydberg excited state. In a manner similar to that described above for the dissociations from species **4** and **5** to form H_2 + OH($X^2\Pi$), the dissociation pathway for species **6** undergoes an avoided crossing (the dashed black line evolves into the dashed green line) in the absence of symmetry to produce OH($A^2\Sigma$) + H_2. This result represents a product which is not accessible from lower-energy H_3O states, and is significant in an experimental context. Under carefully controlled relative beam energies in a heavy-ion storage ring apparatus, it should be possible to select the formation of OH product molecules of a given electronic state. This possibility has not been discussed in the context of the experimental results of $H_3O^+ + e^-$ DR, but is one which should be of considerable interest to experimentalists. Very recent studies by Coe and co-workers of glancing charge transfer reactions of D_3O^+ with H_2O suggest the formation of electronically-excited D_3O and subsequent dissociation to O + D_2 + D.[43]

In addition, OH ($A^2\Sigma$) can be produced by sequential losses of two H atoms as illustrated by the solid red curve in Figure 3. Hence, this second excited state of H_3O should dissociate to produce OH ($A^2\Sigma$) in all cases, should generate no intact H_2O, and can produce both H_2 and 2H. It must be emphasized, however, that species **15** and **16** in Figure 3 do not exist at minima on the H_2O singlet potential energy hypersurface and should not be regarded as reaction intermediates along the dissociation pathways leading to sequential losses of H atoms from **2** and **3**. Thus, the trajectories of these paths should be viewed as leading directly to OH($X^2\Pi$) + 2H and OH($A^2\Sigma$) + 2H, respectively.

The preceding discussions have concentrated primarily on the elucidation of energetically accessible dissociation pathways of ground state and electronically excited H_3O. However, this type of analysis does not address the question of which pathways are preferred immediately upon electron−ion recombination. In an attempt to gain insight into this issue, particularly in the cases of the two lowest-energy valence-to-Rydberg H_3O excited states **2** and **3**, obtained by vertical CIS excitations at the geometry of ground-state H_3O (**1**), we have calculated the forces and nuclear displacements associated with these two molecules as the first steps in their gradient geometric optimizations. While the forces on **2** thus obtained do not provide any useful information in this regard, those on **3** suggest a symmetric dissociation of two H atoms (possibly as H_2) and the retention of an intact O−H moiety, rather than an ejection of a single H atom and retention of H_2O. Thus, the initial forces on **3** appear to favor a symmetric dissociation to OH + H_2 (or to OH + 2 H) via the dashed black line in Figure 3.

The possibility of bond dissociations beyond those observed experimentally (and those studied computationally here) on thermodynamic grounds (as shown in Figure 3) leads us to speculate about the possibility of the formation of other H_3O^+ + e^- DR products, particularly in the presence of a significant amount of excess kinetic energy on initial electron−ion recombination. As was mentioned earlier, the solid blue curve in Figure 3 denotes a sequential loss of H atoms from ground-state $(H_3O)_R$; first to H_2O (X^1A_1) + H, then to OH($X^2\Pi$) + H + H. In addition to this path, as well as the other routes to these products shown in Figure 3, it is also conceivable that, as OH($X^2\Pi$) + H + H lies 36 kcal mol^{-1} below H_3O^+, these products could be formed from OH($X^2\Pi$) + H_2 by H−H bond rupture under appropriate experimental conditions.

IV. Summary

We have performed ab initio MO calculations on potential energy surfaces which connect ground electronic state H_3O and the two lowest valence-to-Rydberg excited-state H_3O species with their respective dissociation products, to gain insight into the intricacies of the formation of experimentally observed products of H_3O^+ + e^- DR. Our investigation has yielded the following results:

(1) Ground-electronic state H_3O, produced by DR of H_3O^+ + e^- at low relative beam energies, can dissociate via several pathways to form $H_2O(X^1A_1)$ + H, OH($X^2\Pi$) + H_2, or OH($X^2\Pi$) + 2H. Although the reaction leading to the first products is the most exothermic, it does not constitute the product channel of largest branching ratio as observed experimentally. We believe that the presence of sufficient excess internal energy in the nascent $H_2O(X^1A_1)$ causes a large fraction of this species to undergo further dissociation to OH ($X^2\Pi$) + H, thereby enhancing the branching ratio of the latter product.

(2) The undulations observed in the experimental reaction cross-section plot at higher relative beam energies may be attributable to the formation of electronically excited valence-to-Rydberg H_3O species on initial recombination. The dissociation pathways (and, in some cases, the products) associated with these states are energetically inaccessible from ground-state H_3O (e.g., OH($A^2\Sigma$)). In this context, then, further investigations of H_3O^+ + e^- DR, with an emphasis on the processes associated with excited states of H_3O, may be of interest to experimentalists, both from the perspective of the nature of the product molecules formed as well as the nature of their branching ratios.

(3) The ground electronic state H_3O dissociates to produce OH($X^2\Pi$) as does the first-excited valence-to-Rydberg H_3O, but the second-excited valence-to-Rydberg H_3O dissociates to produce OH($A^2\Sigma$). Therefore, it may be possible to choose the electronic state of product OH molecules formed under ASTRID conditions by carefully controlling the relative electron-beam to ion-beam energy.

Acknowledgment. This work was supported by NSF Grant No. CHE9618904. We also thank the Utah Center for High Performance Computing for staff resources, as well as an anonymous referee for bringing the research of Ref. 40(c) to our attention.

References and Notes

(1) Bates, D. R.; Massey, H. S. W. *Proc. R. Soc. London Ser. A* **1947**, *192*, 1.

(2) Bates, D. R. *Phys. Rev.* **1950**, *78*, 492.

(3) (a) Bardsley, J. N. *J. Phys. B* **1968**, *1*, 349. (b) Bardsley, J. N. *J. Phys. B* **1968**, *1*, 365.

(4) (a) van Dishoeck, E. F. In *Molecular Astrophysics*, Hartquist, T. W., Ed.; Cambridge University Press: Cambridge, UK, 1990; p 55. (b) Millar, T. J. In *Molecular Astrophysics*; Hartquist, T. W., Ed.; Cambridge University Press: Cambridge, UK, 1990; p 115. (c) Bates, D. R. In *Molecular Astrophysics*; Hartquist, T. W., Ed.; Cambridge University Press: Cambridge, UK, p 211.

(5) Neufeld, D. A.; Lepp, S.; Melnick, G. J. *Astrophys. J. Suppl. Ser.* **1995**, *100*, 132.

(6) See, for example, (a) Bohme, D. K. In *Interaction Between Ions and Molecules*; Ausloos, P., Ed.; Plenum: New York, 1975; p 489. (b) Bohme, D. K.; Mackay, G. I.; Tanner, S. D. *J. Am. Chem. Soc.* **1979**, *101*, 3724. (c) Mackay, G. I.; Tanner, S. D.; Hopkinson, A. C.; Bohme, D. K. *Can. J. Chem.* **1979**, *57*, 1518. (d) Hopkinson, A. C.; Mackay, G. I.; Bohme, D. K. *Can. J. Chem.* **1979**, *57*, 2996. (e) Tanaka, K.; Mackay, G. I.; Bohme, D. K. *Can. J. Chem.* **1978**, *56*, 193. (f) Arsenault, G. P. *J. Am. Chem. Soc.* **1972**, *94*, 8241. (g) Bohme, D. K. In *Kinetics of Ion−Molecule Reactions*; Ausloos, P., Ed.; Plenum: New York, 1979; p 323. (h) Good, A.; Durden, D. A.; Kebarle, P. *J. Chem. Phys.* **1970**, *52*, 222. (i) Mackay, G. I.; Hopkinson, A. C.; Bohme, D. K. *J. Am. Chem. Soc.* **1978**, *100*, 7460. (j) Fehsenfeld, F. C.; Crutzen, P. J., Schmeltekopf, A. L.; Howard, C. J.; Albritton, D. L.; Ferguson, E. E.; Davidson, J. A.; Schiff, H. I. *J. Geophys. Res.* **1976**, *81*, 4454. (k) Fehsenfeld, F. C.; Dotan, I.; Albritton, D. L.; Howard, C. J.; Ferguson, E. E. *J. Geophys. Res.* **1978**, *83*, 1333. (l) Millar, T. J.; Williams, D. A. In *Dust and Chemistry in Astronomy*; Millar, T. J., Williams, D. A., Eds.; Institute of Physics Publishing: Bristol, UK, 1993; p 1. (m) Goodings, J. M.; Ng, C.-W.; Bohme, D. K. *Int. J. Mass Spectrom. Ion Phys.* **1979**, *29*, 57. (n) Goodings, J. M.; Bohme, D. K.; Ng, C.-W. *Combust. Flame* **1979**, *36*, 27. (o) Chen, Q. F.; Milburn, R. K.; Hopkinson, A. C.; Bohme, D. K.; Goodings, J. M. *Int. J. Mass Spectrom.* **1999**, *184*, 153. (p) Goodings, J. M.; Bohme, D. K.; Sugden, T. M. *Sixteenth Symposium (International) on Combustion*. The Combustion Institute: Pittsburgh, PA, 1977; p 891. (q) Spanel, P.; Smith, D. *Int. J. Mass Spectrom.* **1998**, *181*, 1. (r) Goodings, J. M.; Karellas, N. S. *Int. J. Mass Spectrom. Ion Proc.* **1984**, *62*, 199. (s) Hayhurst, A. N.; Telford, N. R. *J. Chem. Soc., Faraday Trans. 1* **1975**, *71*, 1352. (t) Goodings, J. M.; Chen, Q. F. *Can. J. Chem.* **1998**, *76*, 1437. (u) Chen, Q. F.; Goodings, J. M. *Int. J. Mass Spectrom.* **1998**, *181*, 181.

(7) See, for example, (a) Herd, C. R.; Adams, N. G.; Smith, D. *Astrophys. J.* **1990**, *349*, 388. (b) Adams, N. G.; Herd, C. R.; Geoghegan, M. Smith, D.; Canosa, A.; Gomet, J. C.; Rowe, B. R.; Queffelec, J. L.; Morlais, M. *J. Chem. Phys.* **1991**, *94*, 4852. (c) Williams, T. L.; Adams, N. G.; Babcock, L. M.; Herd, C. R.; Geoghegan, M. *Mon. Not. R. Astron. Soc.* **1996**, *282*, 413. (d) Heppner, R.A.; Walls, F. L.; Armstrong, W. T.; Dunn, G. H. *Phys, Rev. A* **1976**, *13*, 1000. (e) Mul, P. M.; McGowan, J. W.; Defrance, P, Mitchell, J. B. A. *J. Phys. B: At. Mol. Phys.* **1983**, *16*, 3099. (f) Mul, P. M.; Mitchell, J. B. A.; D'Angelo, V. S.; Defrance, P.; McGowan, J. W.; Froelich, H. R. *J. Phys. B: At. Mol. Phys.* **1981**, *14*,

1353. (g) Adams, N. G. In *Advances in Gas-Phase Ion Chemistry (Vol. 1)*; Adams, N. G., Babcock, L. M., Eds.; JAI Press: Greenwich, CT, 1992; p 225. (h) Keyser, C. J.; Froelich, H. R.; Mitchell, J. B. A.; McGowan, J. W. *J. Phys. E: Sci. Instrum.* **1979**, *12*, 316. (i) Auerbach, D.; Cacak, R.; Caudano, R.; Gaily, T. D.; Keyser, C. J.; McGowan, J. W.; Mitchell, J. B. A.; Wilk, S. F. J. *J. Phys. B: At. Mol. Phys.* **1977**, *10*, 3797. (j) Hayhurst, A. N.; Telford, N. R. *J. Chem. Soc., Faraday Trans. 1* **1974**, *70*, 1999. (k) Vinkier, C. Ph.D. Dissertation, University of Louvain, 1969. (l) Peeters, J.; Vinkier, C.; van Tiggelen, J. *Oxidation Combust. Rev.* **1969**, *4*, 93. (m) Wilson, L. N.; Evans, E. W. *J. Chem. Phys.* **1967**, *46*, 859. (n) Ogram, G. L.; Chang, J.-S.; Hobson, R. M. *Phys. Rev. A* **1980**, *21*, 982. (o) Wortberg, G. *Tenth Symposium (International) on Combustion*. The Combustion Institute: Pittsburgh, PA, 1965; p 651. (p) Bradley, D.; Mathews, K. J. *Eleventh Symposium (International) on Combustion*. The Combustion Institute: Pittsburgh, PA, 1967; p 359. (q) Kelly, R.; Padley, P. J. *Trans. Faraday Soc.* **1969**, *65*, 355. (r) Semenov, E. S.; Sokolik, A. S. *Zh. Tekh. Fiz.* **1962**, *32*, 1074. (s) Calcote, H. F.; Kurzius, S. C.; Miller, W. J. *Tenth Symposium (International) on Combustion*. The Combustion Institute: Pittsburgh, PA, 1965; p 605. (t) King, I. R. *J. Chem. Phys.* **1961**, *35*, 380. (u) King, I. R. *J. Chem. Phys.* **1957**, *27*, 817. (v) Bell, J. C.; Bradley, D.; Jesch, L. F. *Thirteenth Symposium (International) on Combustion*. The Combustion Institute: Pittsburgh, PA, 1971. (w) Leu, M. T.; Biondi, M. A.; Johnsen, R. *Phys. Rev. A* **1973**, *7*, 292. (x) Lindinger, W. *Phys. Rev. A* **1973**, *7*, 328. (y) Larsson, M. *Annu. Rev. Phys. Chem.* **1997**, *48*, 151. (z) Mitchell, J. B. A. *Phys. Rep.* **1990**, *186*, 215, and references therein.

(8) Adams, N. G.; Herd, C. R.; Smith, D. *J. Chem. Phys.* **1989**, *91*, 963.

(9) Dudeck, M.; Poissant, G.; Rowe, B. R.; Queffelec, J. L.; Morlais, M. *J. Phys. D* **1983**, *16*, 995.

(10) (a) Smith, D.; Adams, N. G. *Adv. At. Mol. Phys.* **1988**, *24*, 1. (b) Adams, N. G.; Smith, D. In *Techniques for the Study of Ion−Molecule Reactions*; Farrar, J. M., Saunders, W. H., Eds.; Wiley: New York, 1988; p 165. (c) Adams, N. G. *Int. J. Mass Spectrom. Ion Proc.* **1994**, *132*, 1, and references therein. (d) Bohme, D. K.; Hemsworth, R. S.; Rundle, H. W.; Schiff, H. I. *J. Chem. Phys.* **1973**, *58*, 3504. (e) Betowski, D.; Payzant, J. D.; Mackay, G. I.; Bohme, D. K. *Chem. Phys. Lett.* **1975**, *31*, 321. (f) Mackay, G. I.; Vlachos, G. D.; Bohme, D. K.; Schiff, H. I. *Int. J. Mass Spectrom. Ion Phys.* **1980**, *36*, 259. (g) Raksit, A. B.; Bohme, D. K. *Int. J. Mass Spectrom. Ion Phys.* **1983**, *55*, 69.

(11) (a) Larsson, M. *Rep. Prog. Phys.* **1995**, *58*, 1267. (b) Larsson, M. *Int. J. Mass Spectrom. Ion Proc.* **1995**, *149/150*, 403. (c) Møller, S. P. In *Conf. Record of the 1991 IEEE Particle Accelerator Conf., San Francisco*; Berkner, K., Ed.; IEEE: New York, 1991; p 2811. (d) Abrahamsson, K.; Andler, G.; Bagge, L.; Beebe, E.; Carlé, P.; Danared, H.; Egnell, S.; Ehrnstén, K.; Engström, M.; Herrlander, C. J.; Hilke, J.; Jeansson, J.; Källberg, A.; Leontein, S.; Liljeby, L.; Nilsson, A.; Paal, A.; Rensfelt, K.-G.; Rosengård, U.; Simonsson, A.; Soltan, A.; Starker, J.; af Ugglas, M.; Filevich, A. *Nucl. Instrum. Methods Phys. Res.* **1993**, *B79*, 269. (e) Tanabe, T.; Noda, K.; Honma, T.; Kodaira, M.; Chida, D.; Watanabe, T.; Noda, A.; Watanabe, S.; Mizobuchi, M.; Yoshizawa, M.; Katayama, T.; Muto, H.; Ando, A. *Nucl. Instrum. Methods Phys. Res.* **1991**, *A307*, 7. (f) Habs, D.; Baumann, W.; Berger, J.; Blatt, P.; Faulstich, A.; Krause, P.; Kilgus, G.; Neumann, R.; Petrich, W.; Stokstad, R.; Schwalm, D.; Szmola, D.; Welti, K.; Wolf, A.; Zwickler, S.; Jaeschke, E.; Krämer, D.; Bisoffi, G.; Blum, M.; Friedrich, A.; Geyer, C.; Grieser, M.; Heyng, H. W.; Holzer, B.; Ihde, R.; Jung, M.; Matl, K.; Ott, W.; Povh, B.; Repnow, R.; Steck, M.; Steffens, E.; Dutta, D.; Kühl, T.; Marx, D.; Schröder, S.; Gerhard, M.; Grieser, R.; Huber, G.; Klein, R.; Krieg, M.; Schmidt, N.; Schuch, R.; Babb, J. F.; Spruch, L.; Arnold, W.; Noda, A. *Nucl. Instrum. Methods Phys. Res.* **1989**, *B43*, 390.

(12) (a) Schmidt, H. T.; Vejby-Christensen, L.; Pedersen, H. B.; Kella, D.; Bjerre, N.; Andersen, L. H. *J. Phys. B.: At. Mol. Opt. Phys.* **1996**, *29*, 2485. (b) Andersen, L. H.; Johnson, P. J.; Kella, D.; Pedersen, H. B.; Vejby-Christensen, L. *Phys. Rev. A* **1997**, *55*, 2799. (c) Larsson, M.; Broström, L.; Carlson, M.; Danared, H.; Datz, S.; Mannervik, S.; Sundström, G. *Physica Scripta* **1995**, *51*, 354. (d) van der Zande, W. J.; Semaniak, J.; Zengin, V.; Sundström, G.; Rosén, S.; Strömholm, C.; Datz, S.; Danared, H.; Larsson, M. *Phys. Rev. A* **1996**, *54*, 5010. (e) Forck, P.; Grieser, M.; Habs, D.; Lampert, A.; Repnow, R.; Schwalm. D.; Wolf, A. *Phys. Rev. Lett.* **1993**, *70*, 426. (f) Forck, P.; Grieser, M.; Habs, D.; Lampert, A.; Repnow, R.; Schwalm, D.; Wolf, A. *Nucl. Instrum. Methods Phys. Res.* **1993**, *B79*, 273. (g) Zajfman, D.; Amitay, Z.; Broude, C.; Forck, P.; Seidel, B.; Grieser, M.; Habs, D.; Schwalm, D.; Wolf, A. *Phys. Rev. Lett.* **1995**, *75*, 814. (h) Tanabe, T.; Katayama, I.; Kamegaya, H.; Chida, K.; Arakaki, Y.; Watanabe, T.; Yoshizawa, M.; Saito, M.; Harayama, Y.; Hosono, K.; Hatanaka, K.; Honma, T.; Noda, K.; Ohtani, S.; Takagi, H. *Phys. Rev. Lett.* **1995**, *75*, 1066. (i) Strömholm, C.; Schneider, I. F.; Sundström, G.; Carata, L.; Danared, H.; Datz, S.; Dulieu, O.; Källberg, A.; af Ugglas, M.; Urbain, X.; Zengin, V.; Suzor-Weiner, A.; Larsson, M. *Phys. Rev. A* **1995**, *52*, R4320. (j) Larsson, M.; Carlson, M.; Danared, H.; Broström, L.; Mannervik, S.; Sundström, G. *J. Phys. B: At. Mol. Opt. Phys.* **1994**, *27*, 1397. (k) Datz, S.; Sundström, G.; Biedermann, C.; Broström, L.; Danared, H.; Mannervik, S.; Mowat, J. R.; Larsson, M. *Phys. Rev. Lett.* **1995**, *74*, 896. (l) Larsson, M.; Danared, H.; Mowat, J. R.; Sigray, P.; Sundström, G.; Broström, L.; Filevich, A.; Källberg, A.; Mannervik, S.; Rensfelt, K. G.; Datz, S. *Phys. Rev. Lett.* **1993**, *70*, 430. (m) Datz, S.; Larsson, M.; Strömholm, C.; Sundström, G.; Zengin, V.; Danared, H.; Källberg, A.; af Ugglas, M. *Phys. Rev. A* **1995**, *52*, 2901. (n) Mowat, J. R.; Danared, H.; Sundström, G.; Carlson, M.; Andersen, L. H.; Vejby- Christensen, L.; af Ugglas, M.; Larsson, M. *Phys. Rev. Lett.* **1995**, *74*, 50. (o) Kella, D.; Johnson, P. J.; Pedersen, H. B.; Vejby-Christensen, L.; Andersen, L. H. *Phys. Rev. Lett.* **1996**, *77*, 2432. (p) Semaniak, J.; Larson, Å.; Le Paddelec, A.; Strömholm, C.; Larsson, M.; Rosén, S.; Peverall, R.; Danared, H.; Djuric, N.; Dunn, G. H.; Datz, S. *Astrophys. J.* **1998**, *498*, 886. (q) Vejby-Christensen, L.; Andersen, L. H.; Heber, O.; Kella, D.; Pedersen, H. B.; Schmidt, H. T.; Zajfman, D. *Astrophys. J.* **1997**, *483*, 531. (r) Andersen, L. H.; Heber, O.; Kella, D.; Pedersen, H. B.; Vejby-Christensen, L.; Zajfman, D. *Phys. Rev. Lett.* **1996**, *77*, 4891.

(13) (a) Roszak, S. *Chem. Phys. Lett.* **1996**, *250*, 187. (b) Halkier, A.; Roberson, M.; Linderberg, J. *Pramana − J. Phys.* **1998**, *50*, 547.

(14) (a) Bates, D. R. *Astrophys. J.* **1986**, *306*, L45. (b) Herbst, E. *Astrophys. J.* **1978**, *222*, 508.

(15) Morgan, T. J.; Berkner, K. H.; Pyle, R. V. *Phys. Rev. Lett.* **1971**, *26*, 602.

(16) GAUSSIAN 94, Revision B.1, Frisch, M. J.; Trucks, G. W.; Schlegel, H. B.; Gill, P. M. W.; Joknson, B. G.; Robb, M. A.; Cheeseman, J. R.; Keith, T.; Petersson, G. A.; Montgomery, J. A.; Raghavachari, K.; Al-Laham, M. A.; Zakrzewski, V. G.; Ortiz, J. V.; Foresman, J. B.; Cioslowski, J.; Stefanov, B. B.; Nanayakkara, A.; Challacombe, M.; Peng, C. Y.; Ayala, P. Y.; Chen, W.; Wong, M. W.; Andres, J. L.; Replogle, E. S.; Gomperts, R.; Martin, R. L.; Fox, D. J.; Binkley, J. S.; Defrees, D. J.; Baker, J.; Stewart, J. P.; Head-Gordon, M.; Gonzalez, C.; Pople, J. A. Gaussian, Inc., Pittsburgh, PA, 1995.

(17) Krishnan, R.; Frisch, M. J.; Pople, J. A. *J. Chem. Phys.* **1980**, *72*, 4244.

(18) Gutowski, M.; Simons, J. *J. Chem. Phys.* **1990**, *93*, 3874.

(19) Schaftenaar, G., MOLDEN 3.4, CAOS/CAMM Center, The Netherlands, 1998.

(20) Schlegel, H. B. *J. Comput. Chem.* **1982**, *3*, 214.

(21) (a) Roothaan, C. C. J. *Rev. Mod. Phys.* **1951**, *23*, 69. (b) Hall, G. G. *Proc. R. Soc. London Ser. A* **1951**, *205*, 541.

(22) (a) Roothaan, C. C. J. *Rev. Mod. Phys.* **1960**, *32*, 179. (b) Binkley, J. S.; Pople, J. A.; Dobosh, P. A. *Mol. Phys.* **1974**, *28*, 1423.

(23) (a) Møller, C.; Plesset, M. S. *Phys. Rev.* **1934**, *46*, 618. (b) Binkley, J. S.; Pople, J. A. *Int. J. Quantum Chem.* **1975**, *9*, 229.

(24) (a) Head-Gordon, M.; Pople, J. A.; Frisch, M. J. *Chem. Phys. Lett.* **1988**, *153*, 503. (b) Frisch, M. J.; Head-Gordon, M.; Pople, J. A. *Chem. Phys. Lett.* **1990,** *166*, 275. (c) Frisch, M. J.; Head-Gordon, M.; Pople, J. A. *Chem. Phys. Lett.* **1990,** *166*, 281. (d) Saebo, S.; Almlöf, J. *Chem. Phys. Lett.* **1989**, *154*, 83.

(25) (a) Banerjee, A.; Adams, N.; Simons, J.; Shepard, R. *J. Phys. Chem.* **1985**, *89*, 52. (b) Simons, J.; Jørgensen, P.; Taylor, H.; Ozment, J. *J. Phys. Chem.* **1983**, *87*, 2745. (c) Cerjan, C. J.; Miller, W. H. *J. Chem. Phys.* **1981**, *75*, 2800. (d) Baker, J. *J. Comput. Chem.* **1986**, *7*, 385. (e) Baker, J. *J. Comput. Chem.* **1987**, *8*, 563.

(26) Gonzalez, C.; Schlegel, H. B. *J. Chem. Phys.* **1989**, *90*, 2154.

(27) (a) Schlegel, H. B. *J. Phys. Chem.* **1988**, *92*, 3075. (b) Schlegel, H. B. *J. Chem. Phys.* **1986**, *84*, 4530.

(28) (a) Pople, J. A.; Binkley, J. S.; Seeger, R. *Int. J. Quantum Chem. Symp.* **1976**, *10*, 1. (b) Morse, P. M.; Feshbach, H. *Methods of Theoretical Physics (Vol. 2)*. McGraw-Hill: New York, 1953; p 1119.

(29) (a) Krishnan, R.; Frisch, M. J.; Pople, J. A. *J. Chem. Phys.* **1980**, *72*, 4244. (b) Krishnan, R.; Pople, J. A. *Int. J. Quantum Chem.* **1978**, *14*, 91. (c) Frisch, M. J.; Krishnan, R.; Pople, J. A. *Chem. Phys. Lett.* **1980**, *75*, 66.

(30) (a) Cizek, J. *J. Chem. Phys.* **1966**, *45*, 4256. (b) Cizek, J. *Adv. Chem. Phys.* **1969**, *14*, 35. (c) Cizek, J.; Paldus, J. *Int. J. Quantum Chem.* **1971**, *5*, 359. (d) Paldus, J.; Cizek, J.; Shavitt, I. *Phys. Rev. A* **1972**, *5*, 50. (e) Bartlett, R. J. *J. Phys. Chem.* **1989**, *93*, 1697. (f) Bartlett, R. J. *Theor. Chim. Acta* **1991**, *80*, 71. (g) Bishop, R. F. *Theor. Chim. Acta* **1991**, *80*, 95. (h) Kutzelnigg, W. *Theor. Chim. Acta* **1991**, *80*, 349. (i) Pople, J. A.; Krishnan, R.; Schlegel, H. B.; Binkley, J. S. *Int. J. Quantum Chem.* **1978**, *14*, 545. (j) Bartlett, R. J.; Purvis, G. D. *Int. J. Quantum Chem.* **1978**, *14*, 561. (k) Purvis, G. D., III.; Bartlett, R. J. *J. Chem. Phys.* **1982**, *76*, 1910. (l) Raghavachari, K.; Trucks, G. W.; Pople, J. A.; Head-Gordon, M. *Chem. Phys. Lett.* **1989**, *157*, 479. (m) Scuseria, G. E.; Lee, T. J. *J. Chem. Phys.* **1990**, *93*, 5851. (n) Watts, J. D.; Cernusak, I.; Noga, J.; Bartlett, R. J.; Bauschlicher, C. W., Jr.; Lee, T. J.; Rendell, A. P.; Taylor, P. R. *J. Chem. Phys.* **1990**, *93*, 8875. (o) Noga, J.; Bartlett, R. J. *J. Chem. Phys.* **1987**, *86*, 7041. (p) Oliphant, N.; Adamowicz, L. *J. Chem. Phys.* **1991**, *95*, 6645. (q) Lee, Y. S.; Kucharski, S. A.; Bartlett, R. J. *J. Chem. Phys.* **1984**, *81*, 5906. (r) Lee, Y. S.; Kucharski, S. A.; Bartlett, R. J. *J. Chem. Phys.* **1985**, *82*, 5761. (s) Noga, J.; Bartlett, R. J.; Urban, M. *Chem. Phys. Lett.* **1987**, *134*, 126. (t) Scuseria, G. E.; Schaefer, H. F., III. *Chem. Phys. Lett.* **1988**, *152*, 382. (u) Kucharski, S. A.; Bartlett, R. J. *Chem. Phys. Lett.* **1989**, *158*, 550.

(v) Scuseria, G. E.; Scheiner, A. C.; Lee, T. J.; Rice, J. E.; Schaefer, H. F., III. *J. Chem. Phys.* **1987**, *86*, 2881. (w) Scuseria, G. E.; Janssen, C. L.; Schaefer, H. F., III. *J. Chem. Phys.* **1988**, *89*, 7382.

(31) The scale factor of 0.95 appropriate to our augmented basis was derived from that prescribed for MP2(full)/6-311G(d,p) (Rodriquez, C. F.; Bohme, D. K.; Hopkinson, A. C. *J. Phys. Chem.* **1996**, *100*, 2942) of 0.94. The ZPE values of six compounds relevant to the present study (H_3O^+, H_2O, $OH(^2\Pi)$, $OH(^2\Sigma)$, and two nonmimimum critical points) were calculated at two levels of theory: MP2(full)/6−311G(d, p), and MP2-(full) with the diffuse-function-augmented basis set described in Section II of this paper. The average ratio of ZPE values for these compounds was found to be 0.98997; dividing 0.94 by this number yielded 0.94952, which we have rounded to 0.95. The relative energies for species **15** and **16**, shown in Figure 3, were calculated at the (CIS/SCF) level of theory with our augmented basis set, with ZPE values derived from the prescribed value of 0.89 at HF/6-31G(d) (Defrees, D. J.; McLean, A. D. *J. Chem. Phys.* **1985**, *82*, 333). The ZPE values of H_2O (X^1A_1), optimized at the RHF level of theory with our augmented basis set and at 6-31G(d), were calculated. The ratio of ZPE values was found to be 1.00252; dividing 0.89 by this number yielded 0.88776, which we have rounded to 0.89.

(32) (a) Foresman, J. B.; Head-Gordon, M.; Pople, J. A.; Frisch. M. J. *J. Phys. Chem.* **1992**, *96*, 135. (b) Foresman, J. B.; Schlegel, H. B. In *Molecular Spectroscopy: Recent Experimental and Computational Advances*; Fausto, R., Ed.; Kluwer Academic: Dordrecht, The Netherlands, 1993; p 11.

(33) (a) Boldyrev, A. I.; Simons, J. *J. Chem. Phys.* **1992**, *97*, 4272. (b) Nefedova, V. V.; Boldyrev, A. I.; Simons, J. *Int. J. Quantum Chem.* **1994**, *55*, 441.

(34) Actually, it is likely that DR of $H_3O^+ + e^-$ at low collision energies occurs by (1) first forming H_3O in a highly excited Rydberg orbital lying electronically just below the energy of H_3O^+ but with excess internal vibrational and/or rotational energy, followed by (2) rapid radiationless relaxation to the electronically lowest-energy state, which we refer to as $(H_3O)_R$.

(35) (a) Talbi, D.; Saxon, R. *J. Chem. Phys.* **1989**, *91*, 2376. (b) Niblaeus, K. S. E.; Roos, B. O.; Siegbahn, P. E. M. *Chem. Phys.* **1977**, *25*, 207. (c) Wang, J.; Boyd, R. J. *Can. J. Phys.* **1994**, *72*, 851. (d) Raynor, S.; Herschbach, D. R. *J. Phys. Chem.* **1982**, *86*, 3592. (e) McLoughlin, P. W.; Gellene, G. I. *J. Phys. Chem.* **1992**, *96*, 4396.

(36) (a) Gellene, G. I.; Porter, R. F. *J. Chem. Phys.* **1984**, *81*, 5570. (b) Raksit, A. B.; Porter, R. F. *Int. J. Mass Spectrom. Ion Proc.* **1987**, *76*, 299. (c) Griffiths, W. J.; Harris, F. M.; Beynon, J. H. *Int. J. Mass Spectrom. Ion Proc.* **1987**, *77*, 233. (d) Griffiths, W. J.; Harris, F. M. *Int. J. Mass Spectrom. Ion Proc.* **1987**, *77*, R7. (e) March, R. E.; Young, A. B. *Int. J. Mass Spectrom. Ion Proc.* **1988**, *85*, 237. (f) Williams, B. W.; Porter, R. F. *J. Chem. Phys.* **1980**, *73*, 5598.

(37) See, for example, (a) Simons, J.; Gutowski, M. *Chem. Rev.* **1991**, *91*, 669. (b) Gutowski, M.; Simons, J.; Hernandez, R.; Taylor, H. L. *J. Phys. Chem.* **1988**, *92*, 6179. (c) Begemann, M. H.; Saykally, R. J. *J. Chem. Phys.* **1985**, *82*, 3570. (d) Gruebele, M.; Polak, M.; Saykally, R. J. *J. Chem. Phys.* **1987**, *87*, 3347. (e) Phillips, T. G.; van Dishoeck, E. F.; Keene, J. *Astrophys. J.* **1992**, *399*, 533, and references therein. (f) Wooten, A.; Magnum, J. G.; Turner, B. E.; Bogey, M.; Boulanger, M.; Combes, F.; Encrenaz, P. J.; Gerin, M. *Astrophys. J.* **1991**, *380*, L79.

(38) (a) de Beer, E.; Kim, E. H.; Neumark, D. M.; Gunion, R. F.; Lineberger, W. C. *J. Phys. Chem.* **1995**, *99*, 13627. (b) Andresen, P.; Häusler, H.; Lülf, H. W. *J. Chem. Phys.* **1984**, *81*, 571. (c) Andresen, P.; Aristov, N.; Beushausen, V.; Häusler, D.; Lülf, H. W. *J. Chem. Phys.* **1991**, *95*, 5763. (d) Smith, I. W. M.; Zellner, R. *J. Chem. Soc., Faraday Trans. 2* **1974**, *70*, 1045. (e) Tully, F. P.; Ravishankara, A. R. *J. Phys. Chem.* **1980**, *84*, 3126. (f) Ravishankara, A. R.; Nicovich, J. M.; Thompson, R. L.; Tully, F. P. *J. Phys. Chem.* **1981**, *85*, 2498. (g) Alagia, M.; Balucani, N.; Casavecchia, P.; Stranges, D.; Volpi, G. G. *J. Chem. Phys.* **1993**, *98*, 2459. (h) Alagia, M.; Balucani, N.; Casavecchia, P.; Stranges, D.; Volpi, G. G.; Clary, D. C.; Kliesch, A.; Werner, H.-J. *Chem. Phys.* **1996**, *207*, 389. (i) Warnatz, J. In *Combustion Chemistry*; Gardiner, W. C., Jr., Ed.; Springer: Berlin, 1984; p 197.

(39) (a) Schlegel, H. B.; Sosa, C. *Chem. Phys. Lett.* **1988**, *145*, 329. (b) Walch, S. P.; Dunning, T. H., Jr. *J. Chem. Phys.* **1980**, *72*, 1303. (c) Dunning, T. H., Jr.; Walch, S. P.; Wagner, A. F. In *Potential Energy Surfaces and Dynamics Calculations*; Truhlar, D. G., Ed.; Plenum: New York, 1981; p 329. (d) Dunning, T. H., Jr.; Harding, L. B. In *Theory of Chemical Reactions (Vol. 1)*; Baer, M., Ed.; Plenum: New York, 1981; p 329. (e) Dunning, T. H., Jr.; Harding, L. B.; Bair, R. A.; Eades, R. A.; Shepard, R. L. *J. Phys. Chem.* **1986**, *90*, 344.

(40) (a) Loomis, R. A.; Lester, M. I. *Annu. Rev. Phys. Chem.* **1997**, *48*, 643. (b) Loomis, R. A.; Lester, M. I. *J. Chem. Phys.* **1995**, *103*, 4371. (c) Lester, M. I.; Loomis, R. A.; Schwartz, R. L.; Walch, S. P. *J. Phys. Chem. A* **1997**, *101*, 9195. (d) Wheeler, M. D.; Todd, M. W.; Anderson, D. T.; Lester, M. I. *J. Chem. Phys.* **1999**, *110*, 6732. (e) Anderson, D. T.; Todd, M. W.; Lester, M. I. *J. Chem. Phys.* **1999**, *110*, 11117.

(41) (a) Miller, S. M.; Clary, D. C.; Kliesch, A.; Werner, H.-J. *Mol. Phys.* **1994**, *83*, 405. (b) Kochanski, E.; Flower, D. R. *Chem. Phys.* **1981**, *57*, 217. (c) Offer, A. R.; van Hemert, M. C. *J. Chem. Phys.* **1993**, *99*, 3836.

(42) Hammond, G. S. *J. Am. Chem. Soc.* **1955**, *77*, 334.

(43) Cohen, M. H.; Seitzinger, J.; Tissandier, M. D.; Coe, J. V. *J. Chem. Phys.* **1999**, *110*, 11113.